Supporting Information

Advancing Thermoelectric and Sensing Performance in Constrained GeTe Thin Films

Xiaoyu Sun[1], Shuaihang Hou[2], Zuoxu Wu[1], Jian Wang[1], Zunqian Tang[1], Xingjun Liu[2,3], Jun Mao[2,3], Qian Zhang[2,3,*], and Feng Cao[1,*]

[1] *School of Science, and Ministry of Industry and Information Technology Key Lab of Micro-Nano Optoelectronic Information System, Harbin Institute of Technology, Shenzhen 518055, China*

[2] *School of Materials Science and Engineering and Institute of Materials Genome & Big Data, Harbin Institute of Technology, Shenzhen 518055, China*

[3] *National Key Laboratory of Precision Welding & Joining of Materials and Structures, Harbin 150001, China*

* Corresponding author:

E-mail addresses: caofeng@hit.edu.cn (Feng Cao) and zhangqf@hit.edu.cn (Qian Zhang).

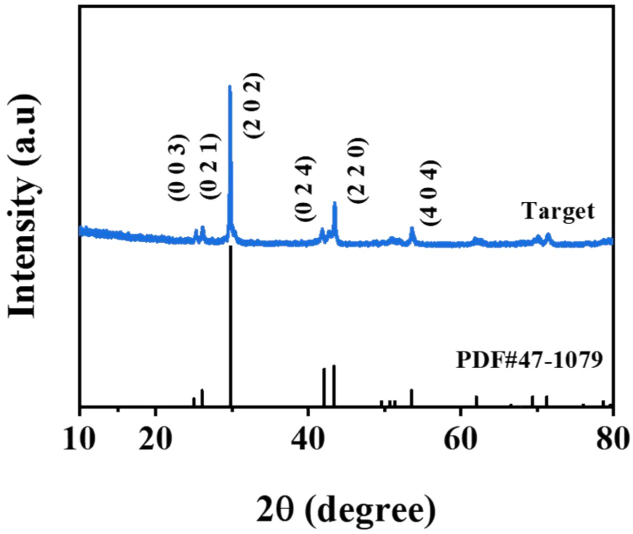

Fig. S1. The XRD pattern of the synthesized GeTe target.

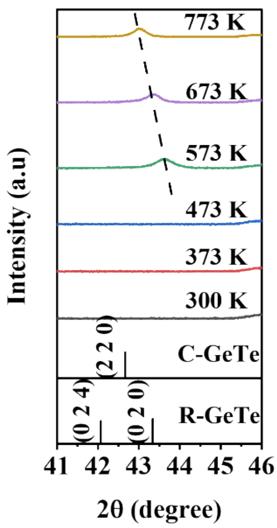

Fig. S2. Temperature dependence of XRD patterns for the GeTe thin film in the 2theta range from 41.0º to 46.0º.

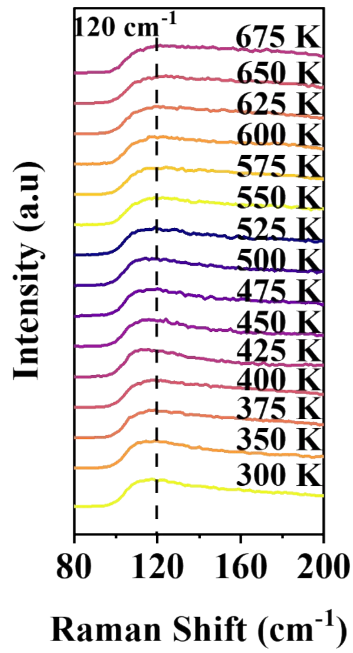

Fig. S3. Temperature dependence of Raman spectroscopy for the GeTe thin film.

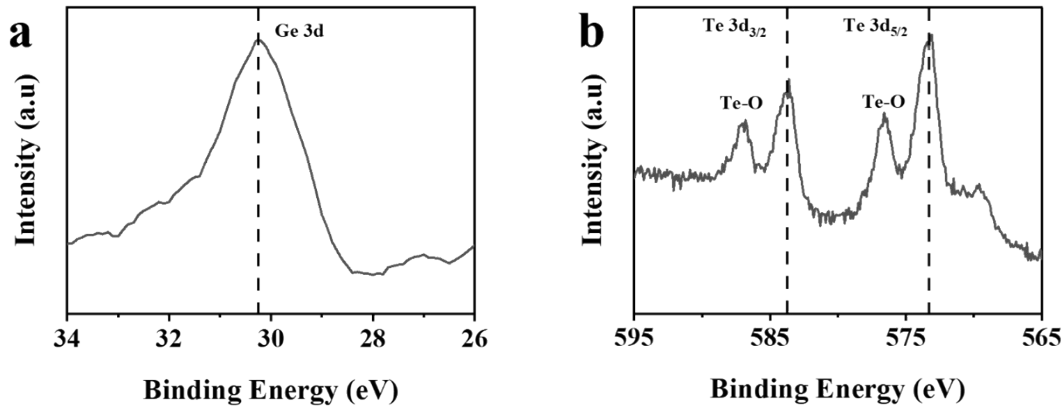

Fig. S4. XPS spectra of (a) Ge and (b) Te. The XPS spectra of the same region clearly shows a new oxidized environment for the tellurium, with distinct appearance of new peaks at binding energies around 576.6 eV (Te-O) and around 586.8 eV (Te-O) due to the HF acid corrosion[1].

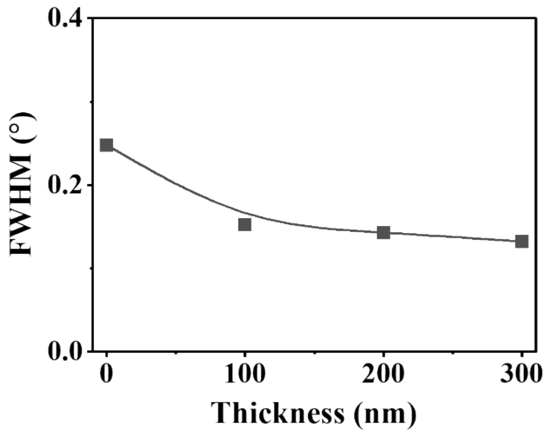

Fig. S5. The full width at half maximum (FWHM) of GeTe films covered with the SiO_2 layer of different thicknesses.

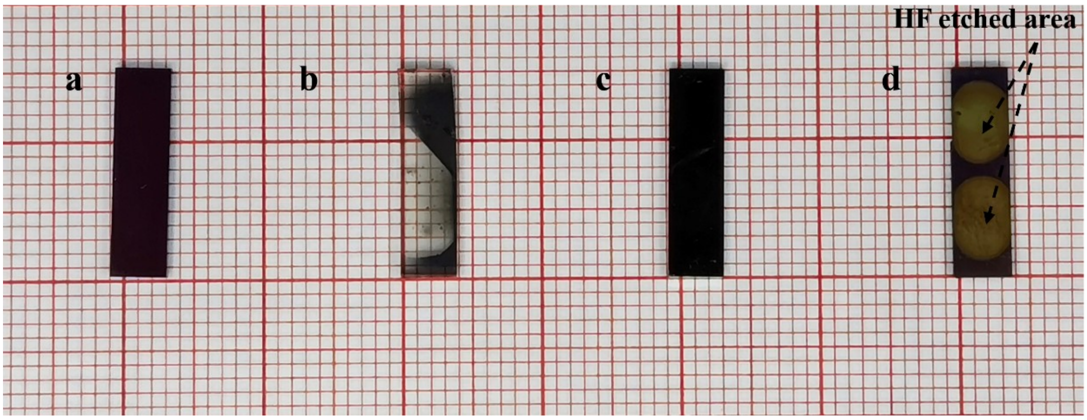

Fig. S6. Optical images of the (a) SiO_2-covered GeTe film without annealing, (b) GeTe film without coving SiO_2 after annealing, (c) SiO_2-covered GeTe film after annealing, (d) SiO_2-covered GeTe film after annealing (HF etched).

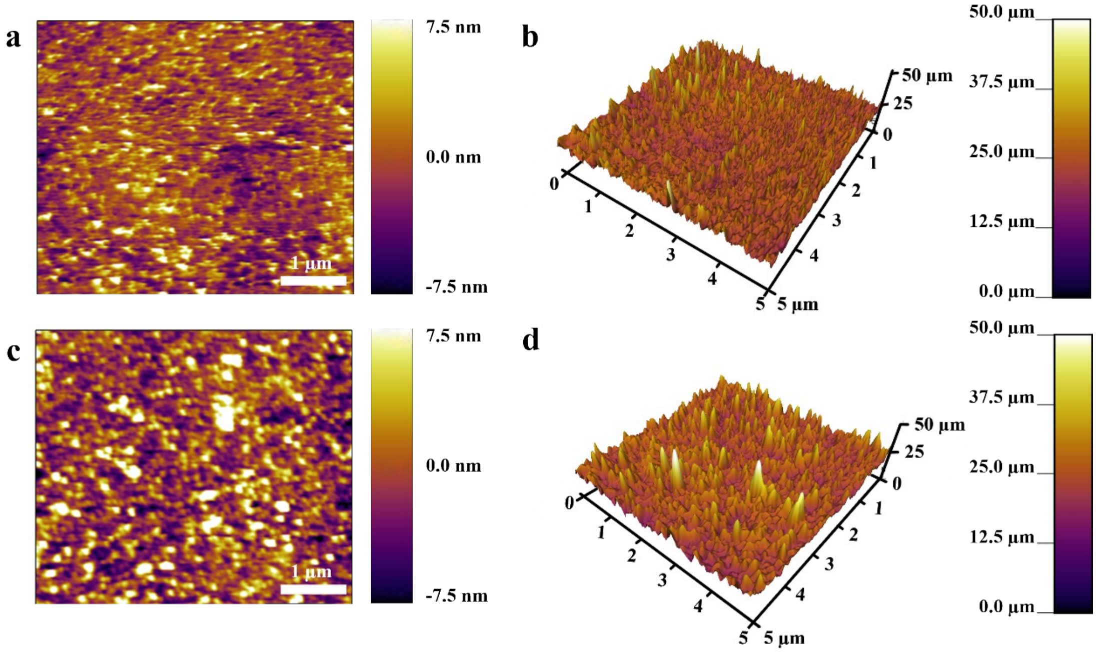

Fig. S7. AFM images (a, b) of the GeTe film before HF etching. AFM images (c, d) of the GeTe film after HF etching.

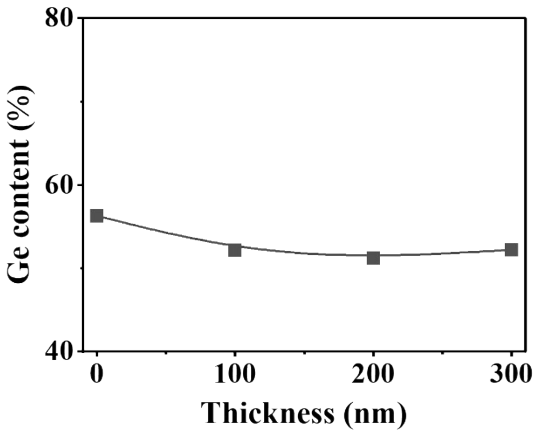

Fig. S8. Element ratio of the GeTe thin films covered with SiO_2 films of different thicknesses.

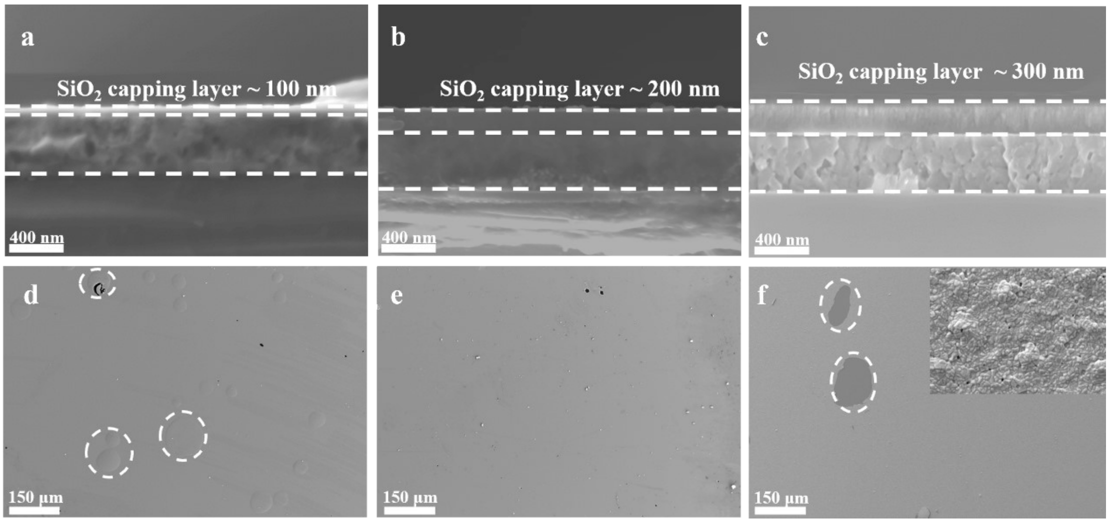

Fig. S9. Cross-sectional SEM images of the GeTe thin film covered with SiO_2 films of different thicknesses (a) 100 nm, (b) 200 nm, (c) 300 nm. Surface morphology of GeTe covered with SiO_2 films of different thicknesses (d) 100 nm, (e) 200 nm, (f) 300 nm.

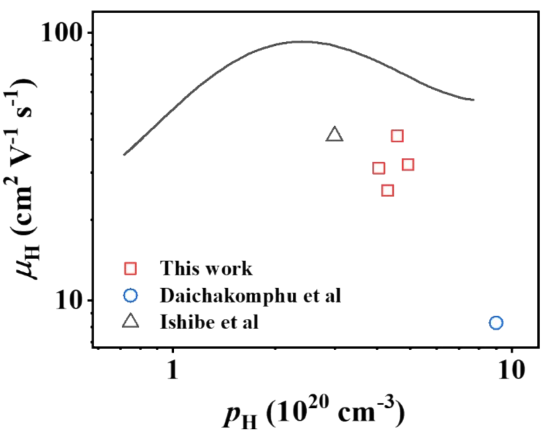

Fig. S10. Carrier concentration dependence of mobility, together with previously reported data. The solid lines are derived from the SPB model with the effective mass of $1.43m_0$.

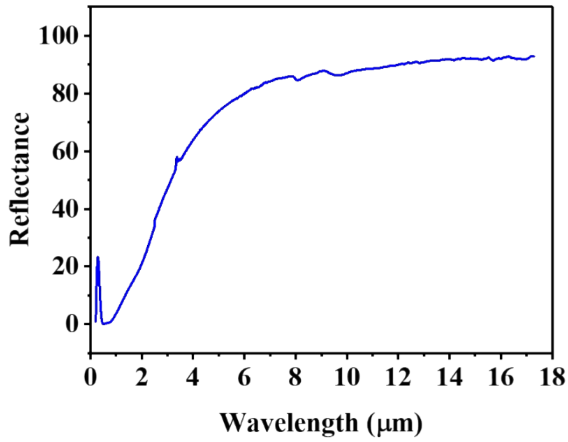

Fig. S11. Reflection spectrum of the solar absorber.

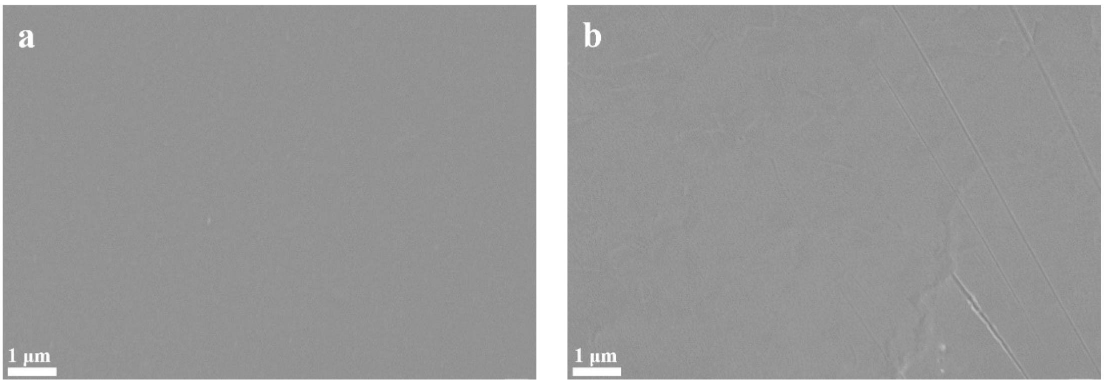

Fig. S12. Surface morphology of (a) W-SiO_2 solar absorber and (b) PDMS/Ag radiation cooler.

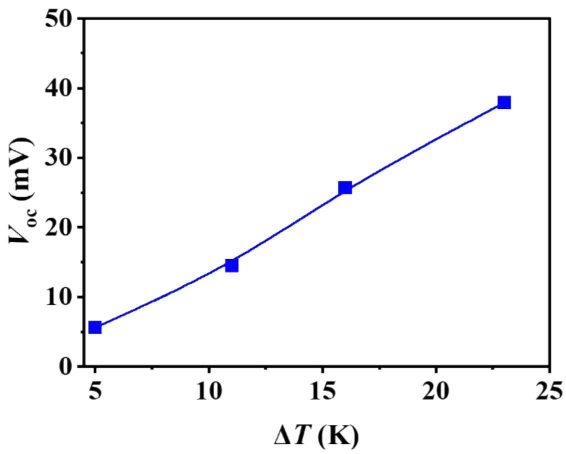

Fig. S13. Simulated open-circuit voltage of TE thin-film device with the diameter 20 mm of the solar absorber under various temperature differences.

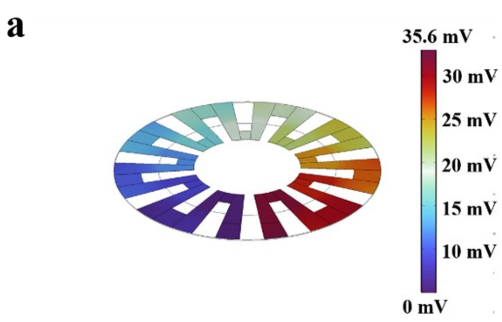

Fig. S14. (a) Simulated open-circuit voltage of the thermoelectric thin film device containing solar absorber under the solar spectrum (AM1.5). (b) Simulated open-circuit voltage of the thermoelectric film device with both solar absorber and radiative cooler under the solar spectrum (AM 1.5).

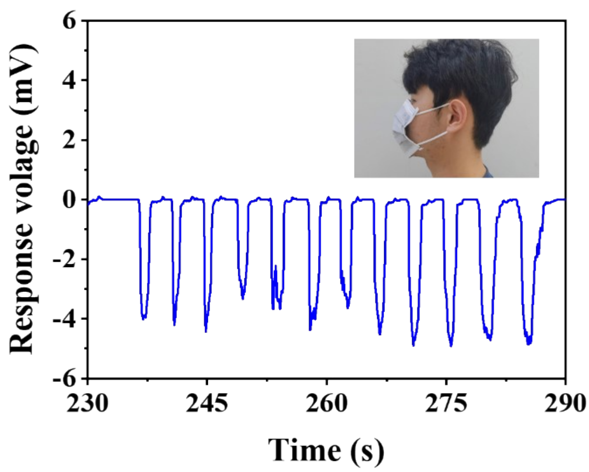

Fig. S15. Voltage response curve of TE thin film device before and after blowing.

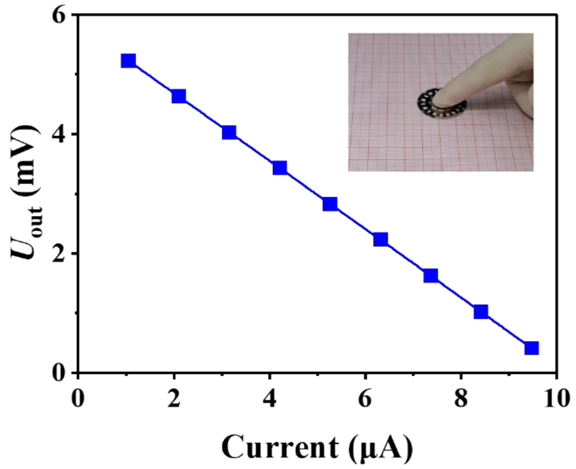

Fig. S16. *I-V* curve of the TE thin film device with touching by the finger.

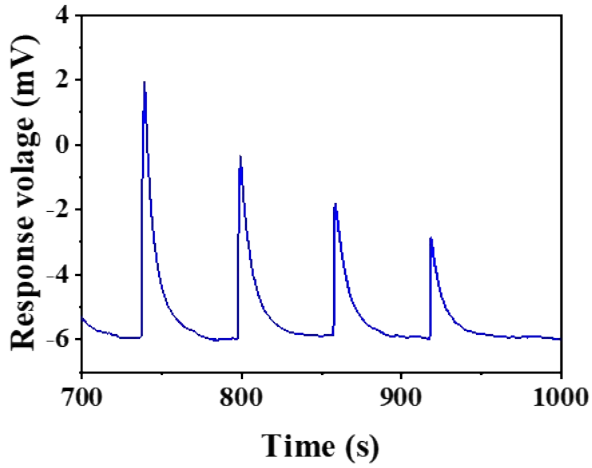

Fig. S17. Voltage response curve of the TE thin film device with touching by the finger.

Table S1. Comparison of thermoelectric devices that can simultaneously harvest radiative cooling and soar heat. The calculated voltages per p-n junction or voltages per device are based on the measured maximum outdoor output voltage.

Thermoelectric materials	Radiative cooler	Solar absorber	Voltage per p-n junction/Voltage per device	Reference
Pt/YIG	GGG	Blackbody paint	0.75 μV	[2]
Bi-Te	PDMS/Al	W/SiO_2	1.04 mV	[3]
Bi-Te/Sb-Te	PDMS/Ag	Polyaniline/anodic aluminum oxide	0.21 μV	[4]
Bi-Te	Poly(L-lactide-co-ε-caprolactone)	PEDOT:PSS or W foil	0.8 mV	[5]
Ag_2Se	PMMA	carbon black/PGMEA	2 mV	[6]
IGZO/CuI	Polyester	Blackbody paint	1.5-2.4 mV	[7]
$GeTe/Ag_2Se$	PDMS/Ag	W/SiO_2	4.3 mV	This work

Supplementary Notes

In order to analyze the impact of environmental climate on thermoelectric devices, a model identical to the actual device was constructed. The model is equipped with a radiation heat transfer module and a solid heat transfer module. The materials properties including the thermal, electrical, and optical performance were obtained from the experimental data. The heat transfer between the TE thin film device and the external environment is simulated using natural convection heat transfer boundary conditions. Parametric scanning was used to set different wind speeds and ambient temperatures to obtain the temperature distribution of the model.

References

1. B. Robert, V. Flaud, R. Escalier, A. Mehdi and C. Vigreux, *Applied Surface Science*, 2023, **607**, 154921.
2. S. Ishii, A. Miura, T. Nagao and K.-i. Uchida, *Science and Technology of Advanced Materials*, 2021, **22**, 441-448.
3. K. Gao, J. Yang, H. Shen, Y. Liu, Y. Li and M. Zhang, *Solar RRL*, 2022, **6**, 2100975.
4. S. Zhang, Z. Wu, Z. Liu, E. Mu, Y. Liu, Y. Lv, T. Thundat and Z. Hu, *Advanced Materials Technologies*, 2022, **7**, 2200478.
5. W. B. Han, S.-Y. Heo, D. Kim, S. M. Yang, G.-J. Ko, G. J. Lee, D.-J. Kim, K. Rajaram, J. H. Lee and J.-W. Shin, *Science Advances*, 2023, **9**, eadf5883.
6. Y. Liu, Q. Zhang, A. Huang, K. Zhang, S. Wan, H. Chen, Y. Fu, W. Zuo, Y. Wang, X. Cao, L. Wang, U. Lemmer and W. Jiang, *Nature Communications*, 2024, **15**, 2141.
7. S. Ishii, C. Bourgès, N. K. Tanjaya and T. Mori, *Materials Today*, 2024.